Probabilistic estimates of future changes in California temperature and precipitation using statistical and dynamical downscaling

David W. Pierce[1,*]

Tapash Das[1,6]

Daniel R. Cayan[1]

Edwin P. Maurer[2]

Norman L Miller[3]

Yan Bao[3]

M. Kanamitsu[1]

Kei Yoshimura[1]

Mark A. Snyder[4]

Lisa C. Sloan[4]

Guido Franco[5]

Mary Tyree[1]

[1]*Scripps Institution of Oceanography, La Jolla, CA*

[2]*Santa Clara University, Santa Clara, CA*

[3]*University of California, Berkeley, Berkeley, CA*

[4]*University of California, Santa Cruz, Santa Cruz, CA*

[5]*California Energy Commission, Sacramento, CA*

[6]*CH2M HILL, Inc., San Diego, CA*

*Corresponding Author address: SIO/CASPO, Mail stop 0224, La Jolla, CA, 92093-0224. dpierce@ucsd.edu, 858-534-8276. Fax: 858-534-8561

Version 2 27 February 2012

ABSTRACT

Sixteen global general circulation models were used to develop probabilistic projections of temperature (T) and precipitation (P) changes over California by the 2060s. The global models were downscaled with two statistical techniques and three nested dynamical regional climate models, although not all global models were downscaled with all techniques. Both monthly and daily timescale changes in T and P are addressed, the latter being important for a range of applications in energy use, water management, and agriculture. The T changes tend to agree more across downscaling techniques than the P changes. Year-to-year natural internal climate variability is roughly of similar magnitude to the projected T changes. In the monthly average, July temperatures shift enough that that the hottest July found in any simulation over the historical period becomes a modestly cool July in the future period. Januarys as cold as any found in the historical period are still found in the 2060s, but the median and maximum monthly average temperatures increase notably. Annual and seasonal P changes are small compared to interannual or intermodel variability. However, the annual change is composed of seasonally varying changes that are themselves much larger, but tend to cancel in the annual mean. Winters show modestly wetter conditions in the North of the state, while spring and autumn show less precipitation. The dynamical downscaling techniques project increasing precipitation in the Southeastern part of the state, which is influenced by the North American monsoon, a feature that is not captured by the statistical downscaling.

1. Introduction

California has a confluence of factors that make it particularly vulnerable to anthropogenically-induced climate change (e.g., Hayhoe et al. 2004, Cayan et al. 2006). Warming and precipitation changes will directly impact crops and pests in the agricultural and wine-producing regions, and affect regional water resources and flood risk through changes in the snow line, snowpack, and evapotranspiration. Indeed, anthropogenic effects can already be seen in the temperature and hydrology of the western U.S. (Barnett et al. 2008, Pierce et al. 2008, Bonfils et al. 2008, Hidalgo et al. 2009, Das et al. 2009; cf. Maurer et al. 2007, who examined a smaller region).

The primary purpose of this work is to present projections of temperature (T) and precipitation (P) change over California by the 2060s in a probabilistic framework (e.g. Manning et al. 2009; Chen et al. 2011), which facilitates risk-based planning and provides a framework for adaptive resource management (e.g., Anderson et al. 2008, Brekke et al. 2009). Global climate models (GCMs; Meehl et al. 2007) do not uniformly sample model uncertainties, and are not independent (Pennell and Reichler, 2011). Therefore the distributions shown here are not true estimates of the probability of future climate changes, rather are best-guess estimates of future climate change given current simulations. We compare our projections of T and P changes to natural internal climate variability, so that the relative magnitude of the two can be assessed.

Spatial downscaling is necessary in California, which is topographically complex. We use daily results from two GCMs dynamically downscaled with three different regional climate models; the same two global models plus two more statistically downscaled on a daily timescale; and the same 4 models plus 12 more (some with multiple ensemble members) statistically downscaled by a different technique on a monthly timescale. In total, we incorporate data from 45 runs originally generated by 16 different global models. The secondary purpose of this work is to compare the climate projections from the dynamical and statistical downscaling techniques and address how they systematically differ. Natural internal climate variability is

included to the extent that the original GCMs simulate it (cf. AchutaRao and Sperber, 2006).

Climate change over California has been extensively studied using some combination of single or multiple GCMs and statistical or dynamical downscaling (e.g., Dickinson et al. 1989; Giorgi et al. 1994; Pan et al. 2001; Kim 2001 and 2005; Snyder et al. 2002; Hayhoe et al., 2004; Leung et al. 2004; Brekke et al. 2004; Maurer and Duffy 2005; Snyder and Sloan 2005; Duffy et al. 2006; Maurer 2007; Liang et al. 2008; Caldwell et al. 2009; Chin et al. 2010). Some common themes emerge from these efforts. First, different GCMs produce different warming and precipitation changes. Second, regional climate models (RCMs) introduce another source of variation, even with the same driving GCM. Third, temperature changes over California are consistently positive, but precipitation changes vary in sign. Fourth, even with the divergent precipitation projections, the effect on California's hydrology is substantial; snowpack declines and runoff shifts to earlier in the water year, with elevation-dependent effects due to the colder temperatures at higher elevations. And fifth, all model simulations exhibit biases, which are assumed to systematically affect the projected climate as well.

Given this body of previous work, it is perhaps surprising that major gaps remain. Few of the studies approached the problem probabilistically, and only Leung et al. 2004, Hayhoe et al. 2004, and Kim 2005 analyze the future daily data, which is critical to energy use, agriculture, ecology, flooding, and water management. Finally, none of the studies used both statistical and dynamical downscaling and compared the two (cf. Hay and Clark 2003, who used both, but over the historical period only and examined runoff rather than T and P). Similar issues have been addressed in other regions; for example, Europe in the PRUDENCE (Christensen et al., 2007) and ENSEMBLES (Kjellstrom and Giorgi, 2010) projects, and the UK with the Climate Projections project (http://ukclimateprojections.defra.gov.uk/).

Pierce et al. (2009) examined 40-year periods over the western U.S., and found that 14 runs developed from 5 global models reliably conveyed the information from the full set of 21 CMIP-3 model results. The bulk of results shown here are generated using monthly data from all 45 runs (developed from 16 global models),

so should be reliable even though the spatial and time scales considered here are somewhat smaller than used in Pierce et al. (2009) (California vs. the western U.S., 10-yr vs. 40-yr periods) and natural internal variability becomes more evident at smaller scales (e.g., Hawkins and Sutton 2010). However the analysis shown here was also done with a subset of 25 runs (excluding multiple ensemble members for any single model) and the results were little different, which suggests that our sampling of available climate model ensemble members is adequate.

Some of our results are from the 9 daily runs developed from 4 global models, which falls short of the ideal number of runs and global models to use. However Pierce et al. (2009) demonstrates that the large majority of the increase in multi-model ensemble averaged skill occurs when going from 1 to 4 global models. We therefore believe that the daily results shown here, obtained from the 9 runs (incorporating information from 4 global models), are both a credible first analysis of the problem and a roadmap showing how the multi-model probabilistic treatment could be extended with additional runs in the future.

2. Data and Methods

We used dynamical downscaling with 3 regional climate models (RCMs): the Regional Climate Model version 3 (RegCM3), which is derived from NCAR's MM5 mesoscale model (Pal et al. 2007); the NCAR/NCEP/FSL Weather Research and Forecasting (WRF) model (Skamarock et al., 2008); and the Regional Spectral Model (RSM, Kanamitsu et al., 2005), which is a regional version of the National Centers for Environmental Prediction (NCEP) global spectral model. Details of the RCMs are given in the Supplemental Material, section 1. Miller et al. (2009) examined the ability of the RCMs used here to simulate California's historical climate when driven with boundary conditions from the NCEP reanalysis II (Kanamitsu et al. 2002), and compared their climatology to observations. That work concluded that all the models have limitations, particularly in parameterized process such as cloud formation, but that "they perform as well as other state-of-the-art downscaling systems, and all do a credible job simulating the historical climate of California" (see also the supplementary information).

We used two methods of statistical downscaling: Bias Correction with Constructed Analogues (BCCA; Hidalgo et al., 2008; Maurer et al. 2010), and Bias Correction with Spatial Disaggregation (BCSD; Wood et al. 2002, 2004) These methods were compared in Maurer and Hidalgo (2008), who concluded that they have comparable skill when downscaling monthly fields of temperature and precipitation. However only BCCA preserves the daily sequence of original global model variability, which is of interest here. Details of the statistical techniques are given in the Supplemental Material, section 2. Some of the BCSD ensemble members were downloaded from the Bias Corrected and Downscaled WCRP CMIP3 Climate Projections archive at http://gdo-dcp.ucllnl.org/downscaled_cmip3_projections (Maurer et al., 2007).

All downscaling is to an approximately a $1/8^{O}$ x $1/8^{O}$ (~ 12 km) spatial resolution. Table 1 lists the various models and number of ensemble members used for each downscaling technique. Not all GCMs were downscaled with all techniques, because of the computer time required and lack of daily data for all the GCMs. Only limited time periods were covered: 1985-94 (the "historical period") and 2060-2069 (the "future period"). Also, only the SRES A2 emissions scenario is used. We note that the 2060s is about the last decade where globally averaged surface temperatures from the A2, B1, and A1B emissions scenarios do not show a clear separation (IPCC 2007). For the dynamical and BCCA downscaling, CMIP-3 ensemble number 1 was used when more than one ensemble member was available.

The 10-year spans are too short to examine natural climate variability from El Nino/Southern Oscillation (ENSO) and the Pacific Decadal Oscillation (PDO) in any one model run. However, we partially make up for this by using 4 to 16 models at a time (depending on the downscaling technique). Natural internal climate variability due to ENSO and the PDO is not synchronized across model runs due to the chaotic nature of the atmosphere. So, for example, one model run might be simulating positive ENSO conditions in model year 2065 while another model run might be simulating negative ENSO conditions. Although both ENSO and the PDO affect California temperature and precipitation, averaging across unsynchronized runs randomly samples different phases of these phenomena, which reduces the net effect of they have on our estimates of anthropogenic

climate change by the 2060's. We do not discard these estimates of natural variability; rather we compare our estimates of anthropogenic climate change to the magnitude of this natural variability so that a better understanding of the relative magnitude of each can be obtained.

Results are presented as averages over the 11 California climate regions identified by Abatzoglou et al. (2009). These regions do a better job representing California's diverse mix of climate regimes than the standard U.S. climate divisions.

2.1 Bias correction

All T and P fields, whether downscaled statistically or dynamically, underwent a bias correction procedure (Panofsky and Brier 1968; Maurer et al. 2002; Wood et al. 2002, 2004; Maurer 2007; Maurer et al. 2010). This is necessary because the project's focus was on hydrological and other applications, and even current state-of-the-art GCMs/RCMs generate T and P fields with biases, often due to biases in the original global fields (e.g., Wood et al. 2004, Duffy et al. 2006, Liang et al. 2008). Details of the bias correction procedure are given in the Supplemental Material, section 3.

3. Results

The probabilistic framework requires that several model runs be included to provide a distribution of projected outcomes. In this work we weight all combinations of global model and downscaling technique equally (except for the multiple ensemble members available from a single global model using BCSD, as described below), following the approach used in the last IPCC assessment (IPCC, 2007). Pierce et al. (2009) looked specifically at the western U.S. and concluded that weighting by model quality does not make a difference to climate projections until after the time period considered here (the 2060s).

BCSD was the only downscaling technique that had multiple downscaled ensemble members available from the same global model (Table 1). When analyzing mean quantities, we combined multiple BCSD downscaled results from

the same global model into a single model mean before analysis, so that each global model contributes equally to the BCSD result despite the disparate number of ensemble members. When computing variability measures this averaging is not appropriate, since averaging reduces the range of variability. In these cases we used a Monte-Carlo approach, constructing 1000 random sets of BCSD results where each model contributed one randomly picked ensemble member. Results shown here are the average obtained across the 1000 random trials. In practice however this makes little difference, as the BCSD results are well sampled even excluding the extra ensemble members.

3.1 Temperature changes

Figure 1 (upper) shows the temperature changes by the 2060s, averaged across all models and downscaling techniques. The yearly-averaged warming is on the order of 2.4 C. The coastal regions experience less warming due to the ocean's moderating influence, with a typical value of about 1.9 C. Inland locations show warming approaching 2.6 C, which may have the potential to suppress coastal warming further via enhanced sea breezes in some locations (Snyder et al. 2003; Lebassi et al. 2009). The lower panels of Fig. 1 show climatological fields for reference.

The mean warming has a pronounced seasonal signature, with the most warming (~3 C) in the summer (June-July-August), and the least warming (< 2 C) in the winter (Dec-Jan-Feb). Since energy use in California is dominated by summer cooling loads rather than winter heating loads, this warming pattern suggests that peak energy use could increase faster than would be expected if only the yearly averaged temperature changes were taken into account.

Figure 2 shows the change in individual monthly distributions of temperature, displayed as a mapping between historic and future percentiles. For example, the blue cross in panel a for the Sacramento/Central valley shows that the 50^{th} percentile temperature in the historical period (x axis) will become the 17^{th} percentile value in the 2060s (y axis). The curves in Fig. 2a start at the origin, which means that the coldest January monthly average temperatures in the historical period will still be experienced in the 2060s. Relative to the evolving

mean, the coldest months become much more dramatic in the future, which might have implications for moving to crops better adapted to hotter conditions. Of the 45 runs (Table 1), 16 have at least one January in the 2060s that is about as cold, or colder, than the coldest historical January in the same model. Despite this, Fig. 2a shows that the median monthly January temperature in the future will be warmer than 8 or 9 out of 10 Januarys today, and the warmest Januarys in the future are completely off the historical distribution.

In July (Fig. 2b), the curves still start nearly at the origin, but inspection showed that such a cold July only existed in two of the 45 runs. On the other hand, the difference in the warmest months is profound. Over most of the state, the warmest monthly average July found in the entire historical distribution of any model is only a 15-40th percentile event in the future period. I.e., a July that is record-breaking hot by current historical standards will become modestly cool in comparison to the new mean.

The yearly warming simulated by the various downscaling techniques is shown in Fig. 3. Results are illustrated for the GFDL 2.1 and CCSM3 global models. Global model results are displayed in Fig. 3f and 3k for comparison. The downscaling techniques generate similar values, and capture the decrease in warming near the coast that is poorly resolved in the global field. BCCA produces a somewhat weaker trend than the other methods for GFDL, although not for CCSM3 (cf. Maurer and Hidalgo (2008), their Fig. 5).

3.1.1 Distributions of seasonal temperature change

The exceedence probability of each year's seasonally averaged temperature change in the future period is shown in Fig. 4. The data in this figure have been re-sampled using the method described in Dettinger (2005), which fleshes out the distributions using a principal component analysis-based resampling technique applied to the variability around the model-mean climate change signal.

Figure 4 shows a distribution composed of one value per year (2060-69) from each model, so each model run contributes 10 values. The values are presented this way to include the effects of interannual natural internal climate variability.

Over most of the domain, there is a 90% chance of experiencing a warming of at least 1 C by the 2060s, and a 10% chance the warming will reach 3-4 C (depending on the season). Although summer (JJA) warming is largest in most of the domain, across the southern regions the differences between the seasons lessens, and autumn (Sep-Oct-Nov, SON) warming matches the JJA warming.

3.1.2 Forced versus natural changes in temperature

The distributions in Fig. 4 have contributions from three sources: 1) the average warming across models; 2) the difference in warming between models; and 3) natural internal climate variability. We estimate each simulation's mean warming as the mean of the 10 yearly values in the future period minus the mean of the 10 values in the historical period. Each simulation's natural internal climate variability is estimated from the difference between the 10 individual yearly values in the future period and the mean of the 10 values in the future period. This method underestimates the true natural internal variability since the 10-yr average in the 2060s will itself be influenced by low-frequency natural variability. The error introduced by this procedure can be estimated from the historical record, as outlined in the supplemental material (Section 4). Errors are modest, on the order of 6-14% (Table SM2, column b). The displayed confidence intervals in Figs. 5 and 9 (blue bars) have been widened by these corrections.

Figure 5 shows the average warming, model spread, and estimate of natural internal climate variability across the 11 climate regions. The annual mean model-estimated warming by the 2060s (Fig. 5a green bars, degrees C) is larger than the 90% confidence interval of natural internal variability (blue bars) in all regions. In practice, this means that the warming will be easily noticeable in the yearly average. The red lines show the 90% confidence interval in estimated warming across the models. The model-to-model variability is small compared to the magnitude of the projected warming. Even if we knew that one of the models used here was perfect and the rest wrong, it would make little difference to the warming estimates.

The seasonal results in Fig. 5 tend to show a larger contribution from natural variability, which is understandable since fewer days are being averaged over.

This is most pronounced in winter (DJF, Fig. 5b), where the typical scale of year-to-year natural fluctuations in seasonally-averaged temperature is roughly twice the expected shift in temperatures. The uncertainly across models (red line) is a larger fraction of the mean warming as well. These tendencies are minimized in summer (JJA, Fig. 5d), where the temperature shifts are as large compared to the natural internal climate variability as seen in the yearly average.

3.1.3 Changes in daily temperature

Only data pooled across the BCCA and dynamical downscaling techniques (which are based on the GCM's daily data) have been used for daily analyses of temperature and precipitation.

Figure 6a shows the cumulative distribution function of daily maximum temperature in July for the historical period (blue) and future period (red). An error function transformation is used on the Y axis, so a Gaussian distribution would form a straight line. All regions show a shift to a higher likelihood of warmer daily maximum temperatures at all probability levels. The shift is smallest at the warmest temperatures in the Northern and central coastal regions, perhaps because of the moderating influence of cool ocean temperatures typically seen in summer along California's coast. Similar curves for daily July minimum temperature display more Gaussian behavior (straighter lines) and lack the reduced warming along the coast (not shown).

By contrast, January daily minimum temperatures (Fig. 6b) show more warming at the highest percentile values and little change below the median. The experience on the ground in January will not be an increase in every day's minimum temperature so much as the appearance of rare days with temperature several degrees warmer than experienced before. While the slopes of the lines in Fig. 6a (July) tend to be the same or slightly steeper in the future, indicating similar or slightly reduced daily variability, the slopes of the lines in Fig. 6b (Jan) tend to be flatter in the future, indicating greater daily variability in projected January daily minimum (and maximum, not shown) temperatures.

Three-day averages of maximum daily temperature in summer (Fig. 7) are of interest to the energy industry, because people are more likely to use air conditioning by the third hot day. The shifts seen here are proportionally much greater than in Fig. 6. Also, in all the inland locations the divergence between the historical and future distribution becomes more pronounced at the warmest temperatures. In the San Joaquin valley, a 3-day run of 40 C or warmer temperatures is only a 1-in-100-yr occurrence in the historical simulations, but is a 1-in-2-yr occurrence in the future simulations. The simulated 3-day average warmest temperature in the Anza-Borrego region is 46 C in the historical era, but 51 C in the future era. Increases along the coast are ~2 C, although even there the incidence of 3-day maximum temperatures with a probability of < 0.01 in the historical era increases by a factor of 10.

3.2 Precipitation changes

The upper panels of Fig. 8 shows the mean precipitation change (%) by the 2060s, averaged across all models and downscaling techniques (45 runs total). Lower panels show climatological fields for comparison. In the annual average (8a), the overall tendency is for small decreases in precipitation in the southern part of the state (< 10%), and negligible changes in the North. The patterns by season are more pronounced, with the northern part of the state experiencing wetter conditions in winter that are nearly offset by drier conditions in the rest of the year. The southern part of the state shows moderate fractional decreases in precipitation in fall, winter and spring but a strong increase in summer precipitation, which will be discussed more below. Bear in mind that California is climatologically dry in the summer, so the large percentage increases found at that time represent small amounts.

3.2.1 Forced versus natural changes in precipitation

Projected changes in seasonal-mean precipitation tend to be small compared to natural internal climate variability (Fig. 9). The blue bars (90% confidence interval of natural variability, tenths of mm/day) are generally an order of magnitude larger than the mean model changes (green bars). At the same time, the spread across the models (red lines) is typically larger than the mean model

change, except for the JJA decrease in precipitation across the northern part of the state (Fig. 9d). However, even precipitation shifts that are small compared to the inter-seasonal or inter-annual variability can be important for the long term water balance of a region, especially where the water supply has little room for reduction. California droughts can last 5-10 years, a long enough averaging period to reduce natural variability sufficiently to expose small but systematic precipitation shifts.

3.2.2 The influence of downscaling technique

The effect of downscaling technique on precipitation must be interpreted cautiously, since not all models were downscaled with all techniques. As a group, the global models downscaled with a daily technique (either dynamical or BCCA) happened to be drier than the average global model by about 10 percentage points in the annual average. In general, the BCCA and dynamical downscaling tend to make the simulation wetter than the original global model field in all regions, typically by about 9-14 percentage points. In the monsoon-influenced region in the southeast of the state this tendency is so strong, the downscaling reverses the sign of the global model projections.

The difference between downscaling techniques can be isolated by using a single global model at a time. Figure 10 shows the yearly precipitation change (%) simulated by the different downscaling techniques applied to the GFDL 2.1 and CCSM3 global model runs, along with the global fields for comparison. The downscaling methods all gave similar results for temperature (Fig. 3). However, for precipitation the agreement depends on the global model. The top row of Fig. 10 shows the different downscaling techniques give similar results when applied to the GFDL 2.1 global model. However the bottom row of Fig. 10 shows that different downscaling methods give quite different results for CCSM3 (i.e., Fig. 10g vs. Fig. 10j), with the statistical methods most similar to the global GCM signal.

The diversity of responses in CCSM3 can be understood, in large part, by considering the details of precipitation changes in each season. Figures 11a and 11b show the statistical downscaling methods applied to CCSM3, while Figs. 11c

and 11d show the dynamical methods. Each panel shows the regions in roughly geographical order, and each region has a set of 4 bars showing the climatological seasonal precipitation in mm (DJF, MAM, JJA, and SON, counting the bars from left to right) and the change in precipitation in mm projected by the downscaling technique (colored portion of the bars). Both dynamical methods show 20-30% precipitation increases in winter, while the statistical methods show increases of less than 10%. Both statistical methods show MAM and SON decreases in precipitation of 20-30%, while the dynamical methods show precipitation decreases of <10%. In other words, the statistical and dynamical downscaling technique are showing the same patterns, but with different weighting by season. Depending on how the oppositely-signed tendencies are weighted, the yearly average difference can be positive or negative.

What determines the differences between a global model trend and the corresponding dynamically downscaled trend? This is addressed in Fig. 12, which shows a selection (DJF and JJA) of seasonally downscaled fields driven by the GFDL and CCSM3 global models. The values plotted are the differences (percentage points) between the dynamically downscaled precipitation changes and the changes found in the original global model. In other words, they are differences of differences, and show not the future precipitation changes, but rather how dynamical downscaling alters the original global model trends. In DJF, the consistencies between the downscaled fields using GFDL (12a, 12e, 12i), and the consistencies between the downscaled fields using CCSM3 (12c, 12g) are greater than the consistencies using the same downscaling technique but a different global model (12a vs. 12c, and 12e vs. 12g). This suggests that in DJF, the effect of dynamical downscaling is influenced primarily by the global model characteristics (e.g., the large-scale atmospheric circulation), and is less sensitive to the dynamical downscaling model used.

In summer, in the southern half of the state, RSM (12f, 12h) tends to show much wetter changes than the global models (either GFDL or CCSM3), while WRF (12b, 12d) shows much drier changes than the global models (either GFDL or CCSM3). The changes produced by RegCM3 lie in between (12j). This indicates that summer precipitation is influenced more by the particular parameterizations used by an individual dynamical downscaling model than by the global driving

model. In the case of RSM, this is despite the fact that spectral nudging is used to keep the regional model results from diverging too greatly from the original global model fields.

3.2.3 Changes in daily precipitation

Three-day accumulations of precipitation can be used to understand the potential for flooding (e.g. Das et al. 2011), as it typically takes a few days for the soil to saturate during a storm. The distributions of the maximum three-day accumulation in a calendar year are shown in Fig. 13. Nearly all of California shows striking increases in maximum three-day accumulations, in many instances generating values far outside the historical distribution. Similar results were found in Kim (2005), although that work considered snow/rain distinctions that we are not examining here. Along the Northern coast, the historical distribution tops out at 80 mm/day with a 0.01/year chance. In the future, that same value has a greater than 0.1/year chance, and the distribution now extends up to 120 mm/day.

For planning purposes it can be useful to know whether the distributions of temperature and precipitation change are related. For example, perhaps the warmest projections are also the driest. However, we find no evidence that the changes in temperature and precipitation distributions are linked in any season.

4. Summary and Conclusions

Our purpose has been to present probabilistic projections of temperature (T) and precipitation (P) changes in California by the 2060s. We have included daily distributions, since a number of important applications in energy demand, water management, and agriculture require daily information. We focused on probabilistic estimates and included natural internal climate variability, because it is useful for planners to understand the range of climate projections and how those compare to natural climate fluctuations.

We downscaled data from 16 global models using a combination of two statistical techniques (BCSD and BCCA) and three nested regional climate models (WRF, RCM, and RegCM3), although not all GCMs were downscaled with all

techniques. In total, we analyzed 9 runs with daily data, plus another 36 with monthly data. As expected, the statistically downscaled fields tend to be closer to the original global model simulations than do the dynamically downscaled fields. All downscaling techniques were combined with equal weighting; exploring the implications of weighting schemes for different downscaling techniques would be a useful future extension of this work. We analyzed a historical (1985-1994) and future (2060-2069) time period, using one emissions scenario, SRES A2. Our estimates of natural internal variability are computed from the available 10-year time slices and adjusted upwards (based on an analysis of observations) to correct for the limited time period included. As appropriate given our focus on applications, all model output was bias corrected.

We find that January-averaged temperatures as cold as any found in the historical period are still seen in the 2060s, although rarer. Januarys warmer than any found in the historical period are seen about 20% of the time. By contrast, cold Julys (judging by current historical standards) nearly disappear by the 2060s, and the hottest July average temperature found in any simulation's historical period becomes a moderately cool event (15-40th percentile) by the 2060s.The warmest Julys are likely to be far outside the historical experience; proportionally, the gain in warm months will be much larger than the loss of cold months.

The downscaled T projections tend to agree across downscaling techniques. Year-to-year variability in seasonally averaged T is about twice as large as the mean seasonal climate warming in winter, and about half the mean warming in summer. In either season, the model range in projected warming is about half the mean warming signal.

Distributions of July daily maximum T shift more or less uniformly towards warmer values, except along the Northern coast, where maximum values are less changed from today. In January, the distributions are little changed below the median, but show a shift towards a greater incidence of a few particularly warm winter days. Distributions of the warmest 3-day average T, which drive air conditioner demand, show approximately uniform shifts of +2 C across the distribution.

Averaged across all models and downscaling techniques, weak annual mean decreases in precipitation are found in the southern part of the state, and near zero P change in the northern part of the state. The disagreement across models is large, however. Winters tend to become wetter in the north, spring and autumn show strong decreases in precipitation, and summer (when the actual values of P are quite small) shows less precipitation in the north but more in the south. Natural variability is typically more than an order of magnitude greater than these seasonally-averaged changes, and the range of projections across models includes zero, except in summer and the southern part of the state in spring.

The different downscaling techniques agree less for annual P changes than they do for T changes. This is due to the annual P change in most models being made up of competing effects, with a tendency towards more winter precipitation and less spring/autumn precipitation. Different models and downscaling techniques weight these competing seasonal effects differently, which can result in a positive or negative change in the yearly average.

The dynamical downscaling techniques show larger increases in summer P in the region affected by the North American monsoon than found with the statistical downscaling techniques. Regional dynamical models are able to amplify monsoon effects that are only coarsely represented by the GCM's, but statistical downscaling has no way to sharpen these features. In general, the winter P response seems more sensitive to which GCM was used, while the summer P response seems more sensitive to which RCM was used. A similar finding was reported in Pan et al. (2001).

There is a substantial increase in 3-day maximum precipitation, with peak values increasing 10-50%, in agreement with Kim (2005). The increases are largest in the northern part of the state, where values that have only a 0.01 probability of occurrence in the historical period become 10 times more likely by the 2060s.

Our results have wide application to the needs of resource managers and other decision makers when adapting to forthcoming climate change in California. In the realm of water management, the pronounced increase in maximum 3-day precipitation accumulation has implications for flooding. Likewise, these results

shed more light on the global model finding that California will generally experience small changes in annual mean precipitation. We show that these small annual mean changes are hiding much larger seasonal changes, with wetter conditions in winter and sharply drier conditions in spring and autumn, although even these seasonal changes are small compared to the natural variability. Generally the simulations suggest that the extreme southeast of the state will experience more summer rainfall as the North American monsoon intensifies, although not all the different downscaling techniques agree as to the magnitude and sign of this response. Probabilistic multi-model climate change evaluations such as those developed here will enable a better understanding of how to adapt to climate change's effects over California.

Acknowledgements

This work was funded by the public interest energy research (PIER) program of the California Energy Commission (CEC), grant 500-07-042 to the Scripps Institution of Oceanography at UC San Diego: Development of probabilistic climate projections for California. We would also like to thank the global modeling groups that contributed data to the CMIP-3 archive; without their efforts and generosity in sharing the data, this work would have been impossible. DWP also received partial support from the International ad-hoc Detection and Attribution (IDAG) project from the US Department of Energy's Office of Science, Office of Biological and Environmental Research, grant DE-SC0004956 and the National Oceanic and Atmospheric Administration's Climate Program Office, and the Department of Energy grant DE-SC0002000 in furtherance of work to examine how daily timescale weather events and the seasonality of precipitation change to accomplish low frequency, global climate changes. Partial salary support for TD from the CALFED Bay-Delta Program funded-postdoctoral fellowship grant is also acknowledged.

References

Abatzoglou JT, Redmond KT, Edwards LM (2009) Classification of Regional Climate Variability in the State of California. J App Meteor Clim 48:1527-1541

AchutaRao K, Sperber KR (2006) ENSO simulation in coupled ocean-atmosphere models: are the current models better? Clim Dyn 27:1-15

Anderson J, Chung F, Anderson M, Brekke L, Easton D, Ejeta M, Peterson R, Snyder R (2008) Progress on incorporating climate change into management of California's water resources. *Climatic Change* **87 (Suppl 1)**:S91–S108, DOI 110.1007/s10584-10007-19353-10581.

Barnett TP, Pierce DW, Hidalgo HG, Bonfils C et al. (2008) Human-induced changes in the hydrology of the western United States. Science 319:1080-1083

Bonfils C, Santer BD, Pierce DW, Hidalgo HG, Bala G, Das T, Barnett TP, Cayan DR, Doutriaux C, Wood AW, Mirin A, Nozawa T (2008) Detection and Attribution of Temperature Changes in the Mountainous Western United States. J Clim 21:6404-6424

Brekke LD, Miller NL, Bashford KE, Quinn NWT, Dracup JA (2004) Climate change impacts uncertainty for water resources in the San Joaquin River Basin, California. J Amer Water Res Assoc 40:149-164

Brekke LD, Maurer EP, Anderson JD, Dettinger MD, Townsley ES, Harrison A, Pruitt T (2009) Assessing reservoir operations risk under climate change, Water Resour. Res., 45, W04411, doi:10.1029/2008WR006941

Caldwell P, Chin HNS, Bader DC, Bala G (2009) Evaluation of a WRF dynamical downscaling simulation over California. Clim Change 95:499-521

Cayan D, Leurs AL, Hanemann M, Granco G, Croes B (2006) Scenarios of climate change in California: An overview. California Climate Change Center report CEC-500-2005-186-SF. 53 pp.

Chen W, Jiang Z (2011) Probabilistic Projections of Climate Change over China under the SRES A1B Scenario Using 28 AOGCMs. J Clim 24:4741-56.

Chin HNS, Caldwell PM, Bader DC (2010) Preliminary Study of California Wintertime Model Wet Bias. Mon Wea Rev 138:3556-3571

Christensen JH, Carter TR, Rummukainen M, Amanatidis G (2007) Evaluating the performance and utility of regional climate models: the PRUDENCE project. Clim Change 81:1-6

559 Das T, Hidalgo H, Cayan DR, Dettinger MD, Pierce DW, Bonfils C, Barnett TP, Bala G, Mirin A
560 (2009) Structure and origins of trends in hydrological measures over the western United States. J
561 Hydromet, **10**:871-892. doi:10.1175/2009JHM1095.1

562 Das T, Dettinger MD, Cayan DR, Hidalgo HG (2011) Potential increase in floods in Californian
563 Sierra Nevada under future climate projections. Clim Change **109** (Suppl 1):S71-94

564 Dettinger MD (2005) From climate-change spaghetti to climate-change distributions for 21st
565 century California. San Francisco Estuary and watershed science. 3:issue 1, article 4. 14 pp

566 Dickinson RE, Errico RM, Giorgi F, Bates GT (1989) A regional climate model for the western
567 United States. Clim Change 15:383-422

568 Duffy PB, Arritt RW, Coquard J, Gutowski W, Han J, Iorio J, Kim J, Leung LR, Roads J, Zeledon
569 E (2006) Simulations of present and future climates in the western United States with four nested
570 regional climate models. J Clim 19:873-895

571 Giorgi F, Brodeur CS, Bates GT (1994) Regional climate-change scenarios over the United States
572 produced with a nested regional climate model. J Clim 7:375-399

573 Hawkins E, Suntton R (2009) The potential to narrow uncertainty in regional climate predicints.
574 Bull Am Met Soc 90:1095-1106.

575 Hay LE, Clark MP (2003) Use of statistically and dynamically downscaled atmospheric model
576 output for hydrologic simulations in three mountainous basins in the western United States. J
577 Hydrol 282:56-75.

578 Hayhoe K, Cayan D, Field CB, Frumhoff PC and others (2004) Emissions pathways, climate
579 change, and impacts on California. Proc Nat Acad Sci 101:12422-12427

580 Hidalgo HG, Dettinger MD, Cayan DR (2008) Downscaling with Constructed Analogues: Daily
581 precipitation and temperature fields over the Unites States. California Energy Commission
582 technical report CEC-500-2007-123. 48 pp.

583 Hidalgo HG, Das T, Dettinger MD, Cayan DR, Pierce DW and others (2009) Detection and
584 Attribution of Streamflow Timing Changes to Climate Change in the Western United States. J
585 Clim 22:3838-3855

586 IPCC (2007) Climate change 2007: The physical science basis. Working group I contribution to
587 the fourth assessment report of the Intergovernmental Panel on Climate Change. Cambridge
588 University Press, Cambridge, United Kingdom and New York, USA. 996 pp.

589 Kanamitsu M, Ebisuzaki W, Woollen J, Yang SK et al. (2002) NCEP-DOE AMIP-II reanalysis
590 (R-2). Bull Am Met Soc 83:1631-1643

591 Kanamitsu M, Kanamaru H, Cui Y, Juang H (2005) Parallel implementation of the regional
592 spectral atmospheric model. California Energy Commission technical report CEC-500-2005-014.
593 www.energy.ca.gov/2005publications/CEC-500-2005-014/CEC-500-2005-014.

594 Kim J (2001) A nested modeling study of elevation-dependent climate change signals in California
595 induced by increased atmospheric CO2. Geophys Res Lett 28:2951-2954

596 Kim J (2005) A projection of the effects of the climate change induced by increased CO2 on
597 extreme hydrologic events in the western US. Clim Change 68:153-168

598 Lebassi, B, González J, Fabris D, Maurer E, Miller N, Milesi C, Switzer P, Bornstein R (2009)
599 Observed 1970–2005 Cooling of Summer Daytime Temperatures in Coastal California. J. Clim
600 **22**:3558-3573.

601 Leung LR, Qian Y, Bian XD, Washington WM, Han JG, Roads JO (2004) Mid-century ensemble
602 regional climate change scenarios for the western United States. Clim Change 62:75-113

603 Liang XZ, Kunkel KE, Meehl GA, Jones RG, Wang JXL (2008) Regional climate models
604 downscaling analysis of general circulation models present climate biases propagation into future
605 change projections. Geophys Res Lett 35 doi:10.1029/2007GL032849

606 Manning LJ, Hall JW, Fowler HJ, Kilsby CG, Tebaldi C (2009), Using probabilistic climate
607 change information from a multimodel ensemble for water resources assessment, Water Resour.
608 Res., 45, W11411, doi:10.1029/2007WR006674

609 Maurer EP, Wood AW, Adam JC (2002) A long-term hydrologically based dataset of land surface
610 fluxes and states for the conterminous United States. J Clim 15:3237-51

611 Maurer EP, Duffy PB (2005) Uncertainty in projections of streamflow changes due to climate
612 change in California. Geophys Res Lett 32, doi:10.1029/2004GL021462

613 Maurer EP (2007) Uncertainty in hydrologic impacts of climate change in the Sierra Nevada,
614 California, under two emissions scenarios. Clim Change 82:309-325

615 Maurer EP, Brekke L, Pruitt T, Duffy PB (2007) Fine-resolution climate change projections
616 enhance regional climate change impact studies, Eos, Transactions, American Geophysical Union,
617 88:504, doi:10.1029/2007EO470006

618 Maurer EP, Stewart IT, Bonfils C, Duffy PB, Cayan DR (2007) Detection, attribution, and
619 sensitivity of trends toward earlier streamflow in the Sierra Nevada, J. Geophy Res 112, D11118,
620 doi:10.1029/2006JD008088

621 Maurer EP, Hidalgo HG (2008) Utility of daily vs. monthly large-scale climate data: an
622 intercomparison of two statistical downscaling methods. Hydrol. Earth Syst. Sci., **12:**551-563.

623 Maurer EP, Hidalgo HG (2010) The utility of daily large-scale climate data in the assessment of
624 climate change impacts on daily streamflow in California. Hydrol. Earth Syst. Sci., **14**:1125-1138,
625 doi:10.5194/hess-14-1125-2010

626 Meehl GA, Covey C, Delworth T, Latif M and others (2007) The WCRP CMIP3 multimodel
627 dataset - A new era in climate change research. Bull Am Met Soc 88:1383

628 Miller NL, Jin J, Schlegel NJ, Snyder MA et al. (2009) An analysis of simulated California climate
629 using multiple dynamical and statistical techniques. California Energy Commission report CEC-
630 500-2009-017-F, August, 2009. 47 pp.

631 Pal JS, Giorgi F, Bi XQ, Elguindi N et al. (2007) Regional climate modeling for the developing
632 world - The ICTP RegCM3 and RegCNET. Bull Amer Met Soc 88:1395

633 Pan Z, Christensen JH, Arritt RW, Gutowski WJ, Takle ES, Otieno F (2001) Evaluation of
634 uncertainties in regional climate change simulations. J Geophys Res Atmos 106:17735-17751

635 Panofsky HA. Brier GW (1968) Some Applications of Statistics to Meteorology, The Pennsylvania State
636 University, University Park, PA, USA, 224 pp.

637 Pennell C, Reichler T (2011) On the Effective Number of Climate Models. J. Clim, 24:2358–2367.
638 doi: 10.1175/2010JCLI3814.1

639 Pierce DW, Barnett TP, Hidalgo HG, Das T et al. (2008) Attribution of Declining Western US
640 Snowpack to Human Effects. J Clim 21:6425-6444

641 Pierce DW, Barnett TP, Santer BD, Gleckler PJ (2009) Selecting global climate models for
642 regional climate change studies. Proc Nat Acad Sci 106:8441-8446

643 Skamarock WC, Klemp JB, Duidhia J, Gill DO, Barker DM, Duda MG, Huang X-Y, Wang W,
644 Powers JG (2008): A description of the Advanced Research WRF Version 3. NCAR technical note
645 NCAR/TN-475+STR. 125 pp.

646 Snyder MA, Bell JL, Sloan LC, Duffy PB, Govindasamy B (2002) Climate responses to a
647 doubling of atmospheric carbon dioxide for a climatically vulnerable region. Geophys Res Lett
648 29:4

649 Snyder MA, Sloan LC, Diffenbaugh NS, Bell JL (2003) Future climate change and upwelling in
650 the California Current. Geophys. Res Lett 30:1823

651 Snyder MA, Sloan LC (2005) Transient future climate over the western United States using a
652 regional climate model. Earth Interactions v. 9 paper 11.

653 Wood AW, Maurer EP, Kumar A, Lettenmaier DP (2002) Long-range experimental hydrologic
654 forecasting for the eastern United States. J Geophys Res Atmos 107 , doi:10.1029/2001jd000659

Wood AW, Leung LR, Sridhar V, Lettenmaier DP (2004) Hydrologic implications of dynamical and statistical approaches to downscaling climate model outputs. Clim Change 62:189-216

Table 1

GCM	Institution	BCSD	BCCA	WRF	RSM	RegCM3
BCCR BCM 2.0	Bjerknes Centre Clim. Res., Bergen, Norway	1				
CCCMA CGCM3.1	Canadian Centre, Victoria, B.C., Canada	5				
CNRM CM3	Meteo-France, Toulouse, France	1	1			
CSIRO MK3.0	CSIRO Atmos. Res., Melbourne, Australia	1				
GFDL CM2.0	Geophys. Fluid Dyn. Lab, Princeton, NJ, USA	1				
GFDL CM2.1	Geophys. Fluid Dyn. Lab, Princeton, NJ, USA	1	1	1	1	1
GISS e_r	NASA/Goddard Inst. Space Studies, N.Y., USA	1				
INMCM 3.0	Inst. Num. Mathematics, Moscow, Russia	1				
IPSL CM4	Inst. Pierre Simon Laplace, Paris, France	1				
MIROC 3.2 medres	Center Climate Sys. Res., Tokyo, Japan	3				
MIUB ECHO-G	Meteor. Inst. U. Bonn, Bonn, Germany	3				
MPI-ECHAM5	Max Planck Inst. Meteor., Hamburg, Germany	3				
MRI CGCM2.3.2	Meteor. Res. Inst., Tsukuba, Ibaraki, Japan	5				
NCAR CCSM3	Nat. Center Atmos. Res., Boulder, CO, USA	4	1	1	1	
NCAR PCM1	Nat. Center Atmos. Res., Boulder, CO, USA	4	1			
UKMO HadCM3	UK Met Office, Exeter, Devon, UK	1				

Table 1. The global general circulation models (GCMs) used in this project, their originating institution, and the number of ensemble members downscaled by the indicated method. BCSD: bias correction with spatial disaggregation; BCCA: bias correction with constructed analogues; WRF: weather research forecast model; RSM: regional spectral model; RegCM3: Regional climate model version 3.

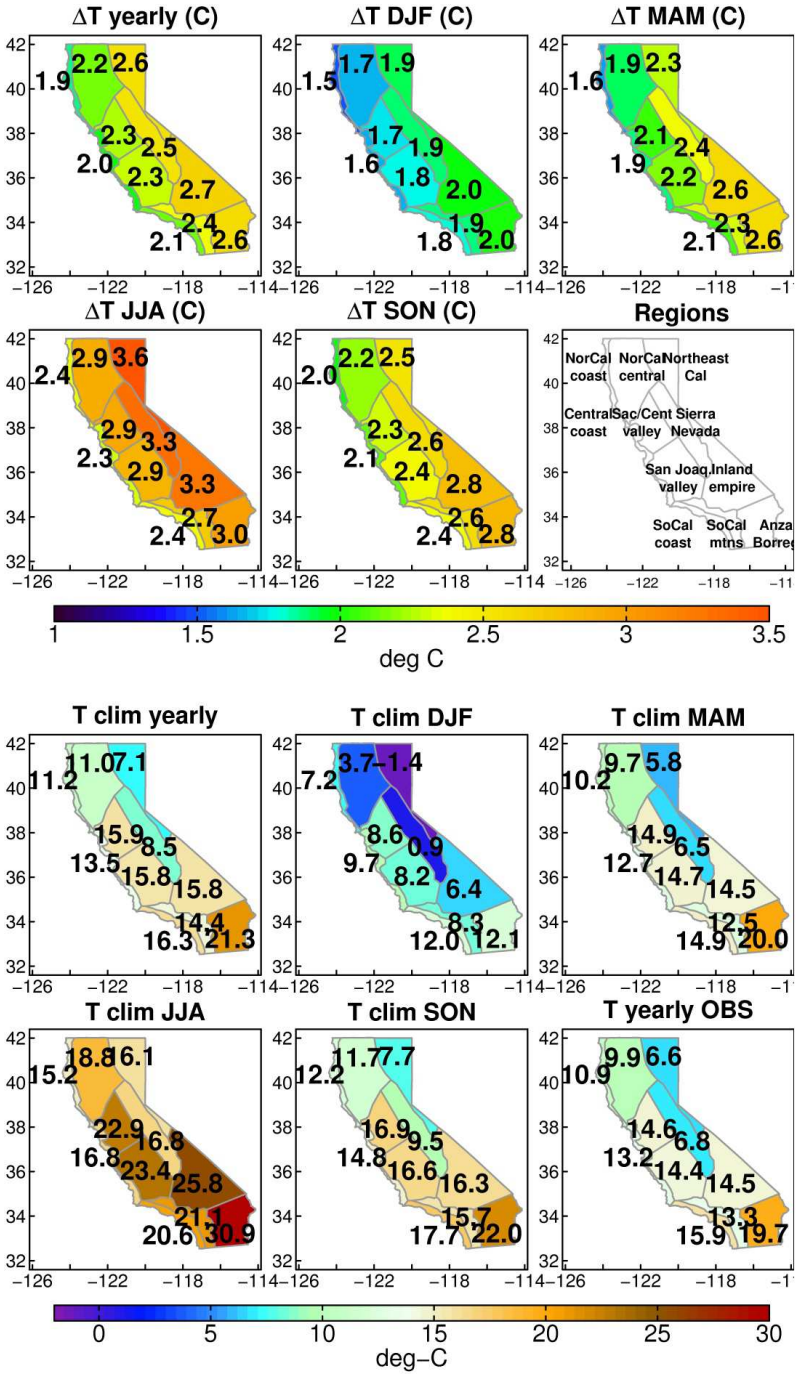

Figure 1. Upper: temperature change (°C) from years 1985-94 to 2060-69. The seasonally-averaged data from all models and downscaling techniques was averaged across models to generate the values. The regions used in this work are also shown. Lower: temperature climatology (°C) averaged across the models, and observed annual mean for comparison (lower right).

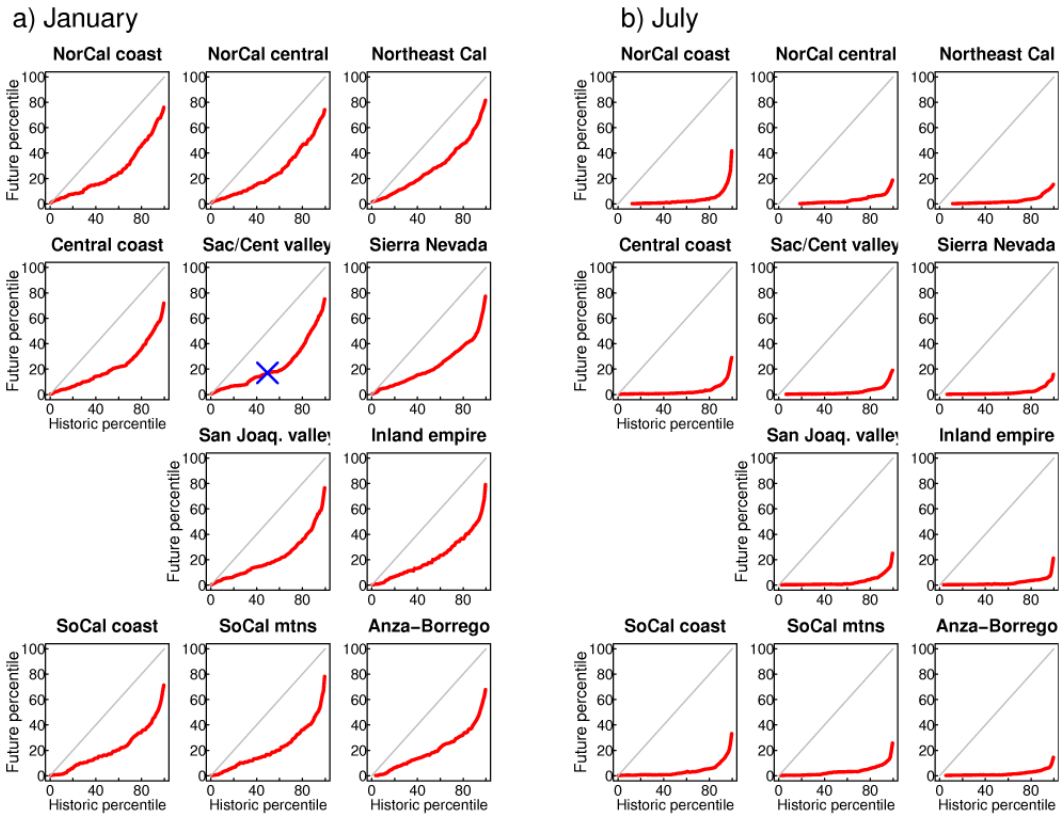

Figure 2. Correspondence between percentiles of monthly-averaged temperature in the historical period (x axis) and future period (y axis), for January (left) and July (right). For instance, the blue cross in panel a for the Sacramento/Central valley shows that the 50th percentile temperature in the historical period will become the 17th percentile value in the 2060s. The grey line shows what the result would be if there were no changes in the distributions. The regions are plotted in roughly geographic order (Northwest locations in the top left, etc.). The figure is made with monthly data from all 45 model runs.

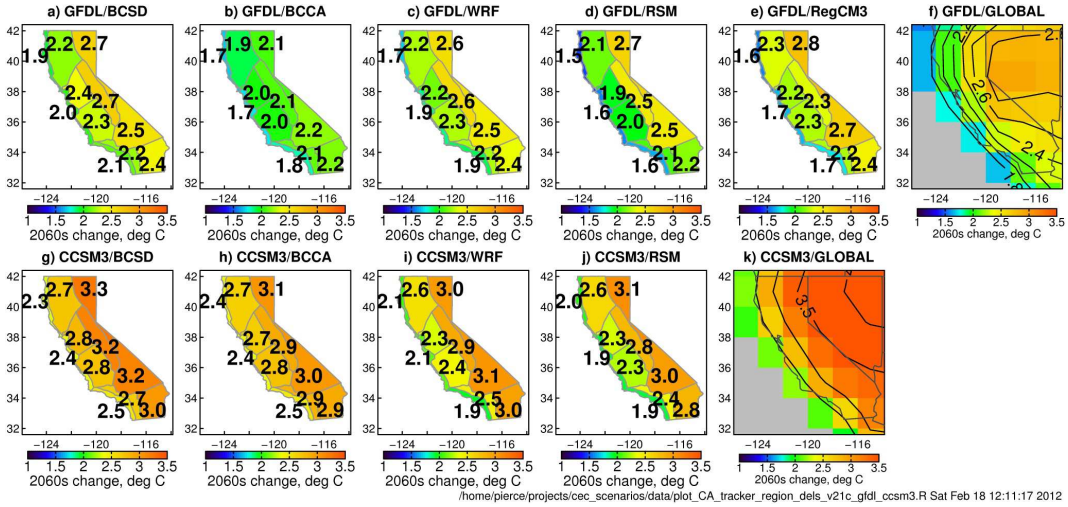

677

678 Figure 3. Yearly temperature change (C) (2060-2069 minus 1985-1994) from each downscaling
679 technique applied to the GFDL 2.1 global model (upper) and CCSM3 global model (lower). The
680 yearly temperature changes from the global models are shown in panels f and k, for comparison.

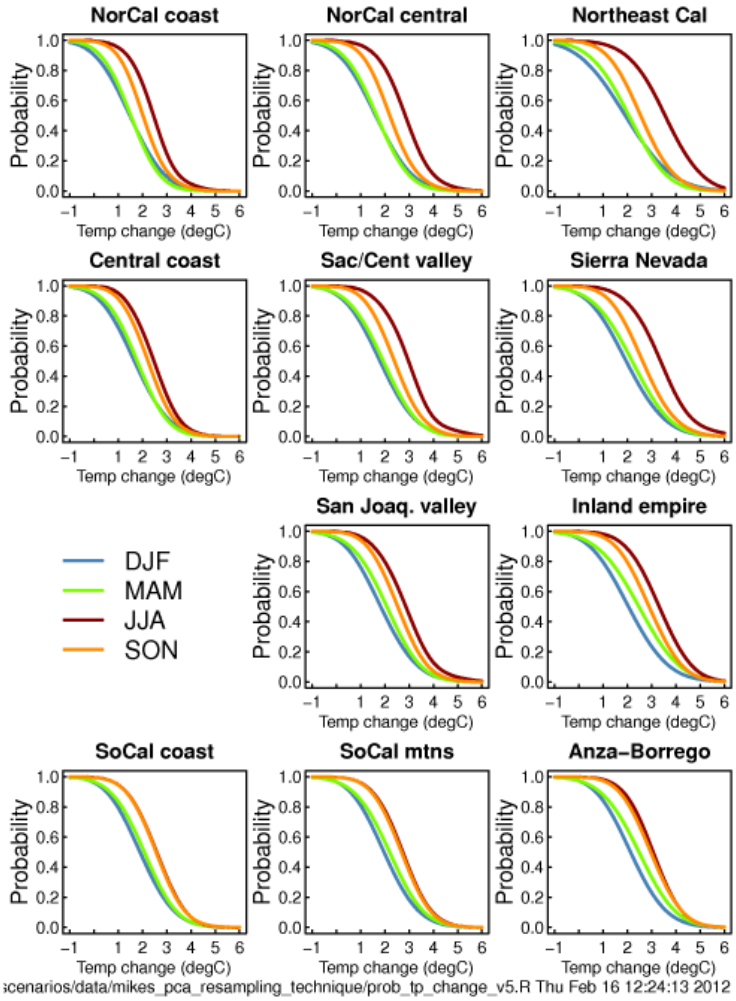

Figure 4. Probability of a temperature change of the indicated value or greater, by region and season. The regions are plotted in roughly geographic order (Northwest locations in the top left, etc.). Monthly data from all 45 runs is used to make the figure.

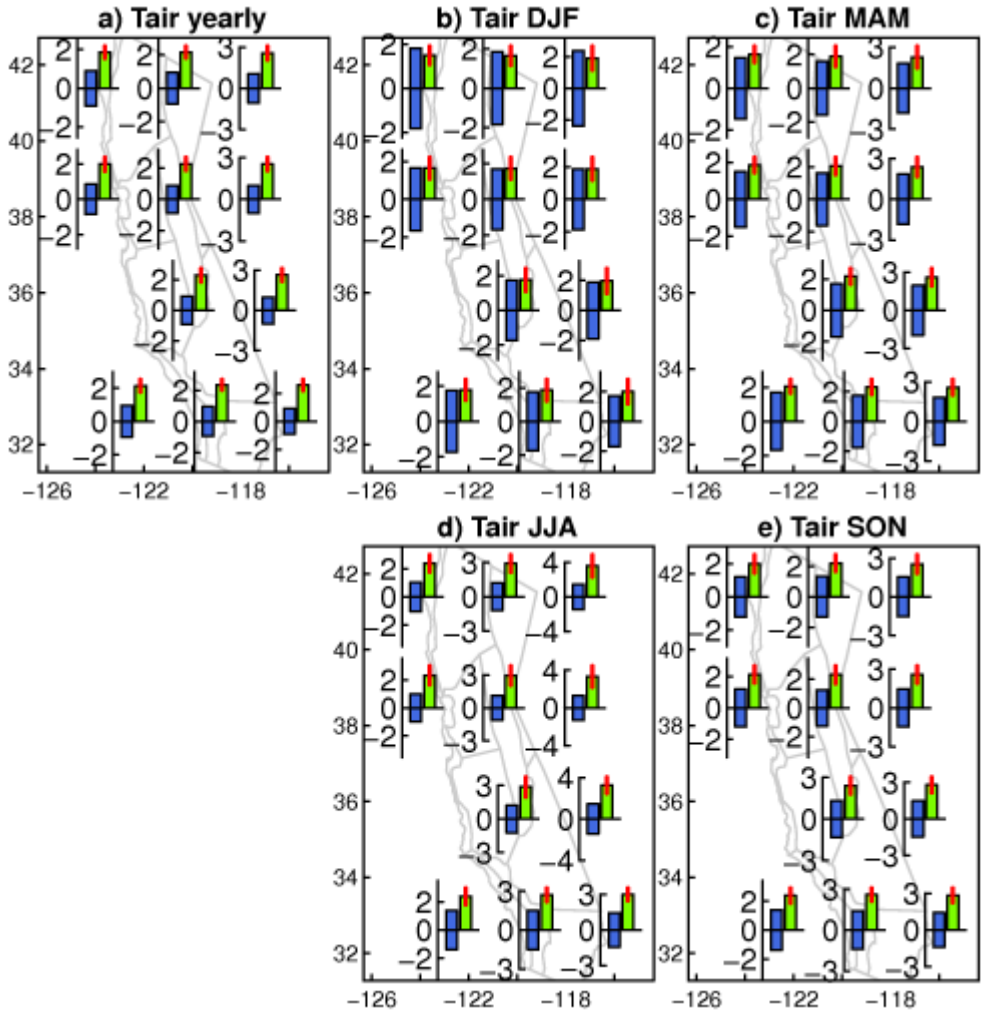

685

686 Figure 5. A comparison of the contribution of natural internal climate variability and model
687 uncertainty to yearly and seasonally averaged projected temperature changes by the 2060s. Blue
688 bars show the 90% confidence interval of natural internal climate variability in near surface air
689 temperature (C) estimated across all models. Green bars show the mean model warming projected
690 in the period 2060-69. The red line shows the 90% confidence interval in the projected warming
691 across models. Note that each inset plot has a different scale for the Y axis, in degrees C. Monthly
692 data from all 45 runs is used to make the figure.

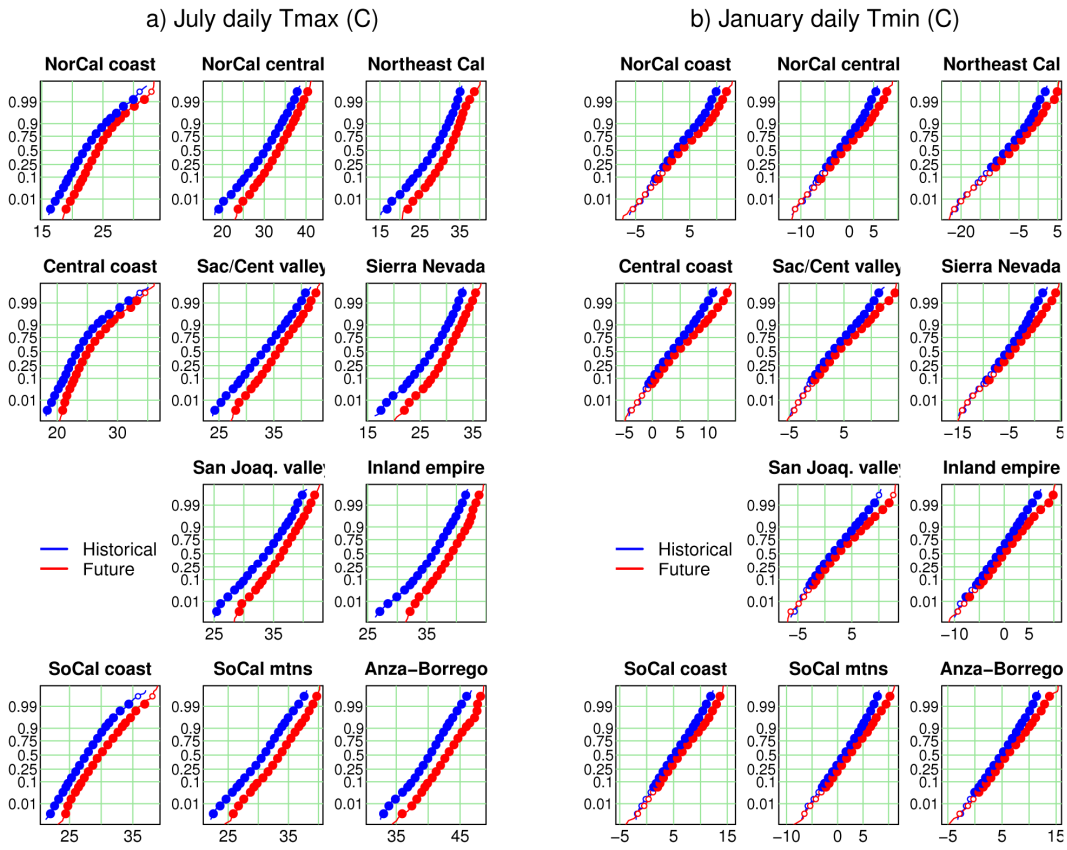

Figure 6. Cumulative distribution functions of July daily maximum temperature (left) and Januray daily minimum temperature (right) across the regions (plotted roughly geographically). The Y axis shows the probability (zero to one) of experiencing the indicated temperature or lower on any particular day. Results from the historical run are in blue; the future run is in red. Large solid dots show where the two curves are different at the 95% significance level, evaluated using a bootstrap technique. Open circles indicate statistically indistinguishable values. Data from the 9 runs with daily data was used to make the figure.

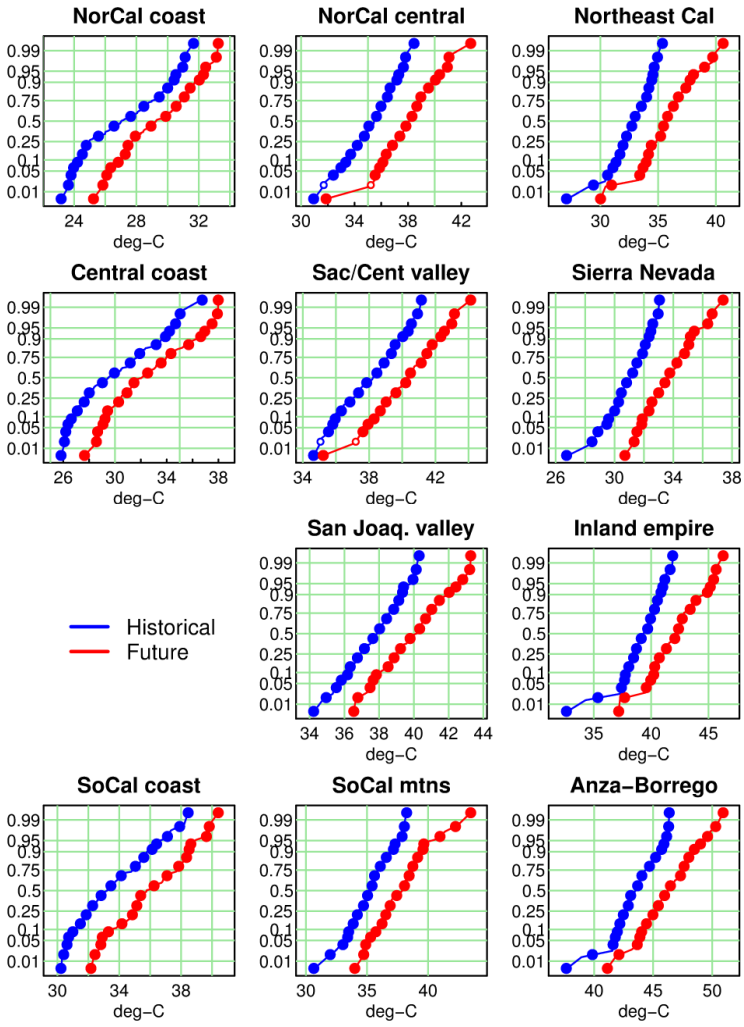

Figure 7. Cumulative distribution functions of the highest 3-day average temperature in the year. The Y axis shows the probability (zero to one) of having the warmest 3 days in a year be the indicated temperature or lower. Results from the historical run are in blue; the future run is in red. Panels are plotted roughly geographically. Large solid dots show where the two curves are different at the 95% significance level evaluated using a bootstrap technique. Data from the 9 runs with daily data was used to make the figure.

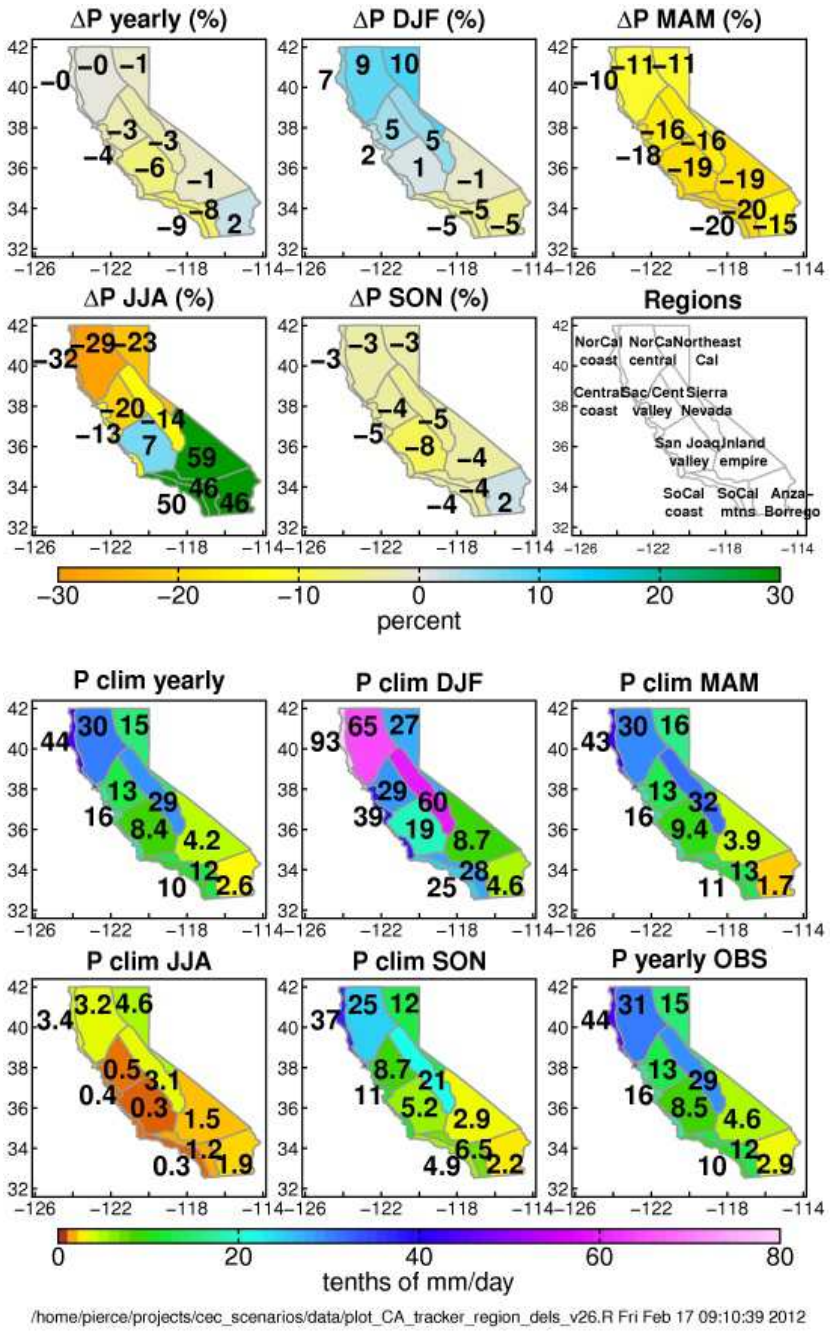

Figure 8. Upper panels: Precipitation change (%), mean over the period 2060-69 compared to mean over the period 1985-94. Data from all models and downscaling techniques was averaged to generate the values. Lower panels: model climatological precipitation (tenths of mm/day), and annual average from observations for comparison (lower right).

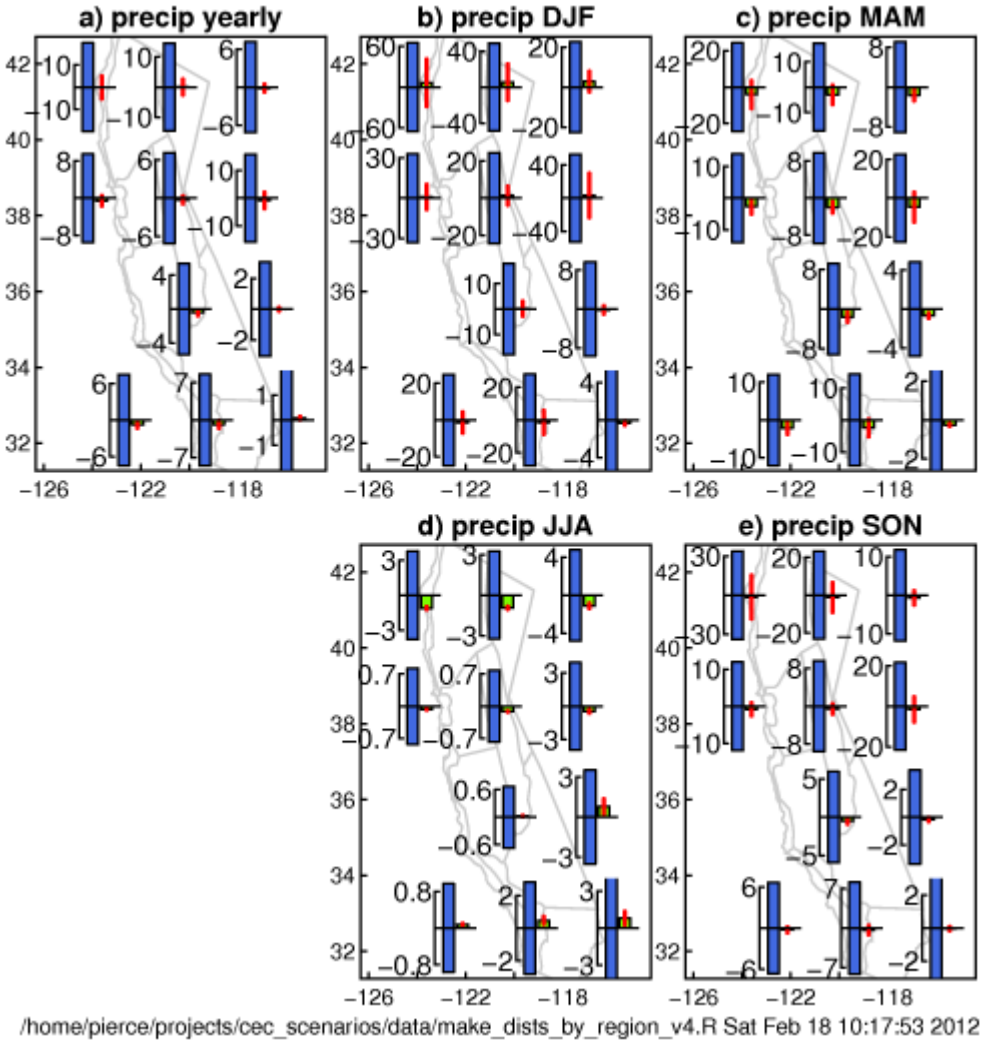

Figure 9. A comparison of the contribution of natural internal climate variability and model uncertainty to yearly and seasonally averaged precipitation changes. Blue bars show the 90% confidence interval of natural internal climate variability in seasonally averaged precipitation (tenths of mm/day) estimated across all models, for the period 2060-69. Green bars show the mean model precipitation change projected in the period 2060-69. The red line shows the 90% confidence interval in the projected precipitation change across models. Note that each inset plot has a different scale for the Y axis. Monthly data from all 45 runs is used to make the figure.

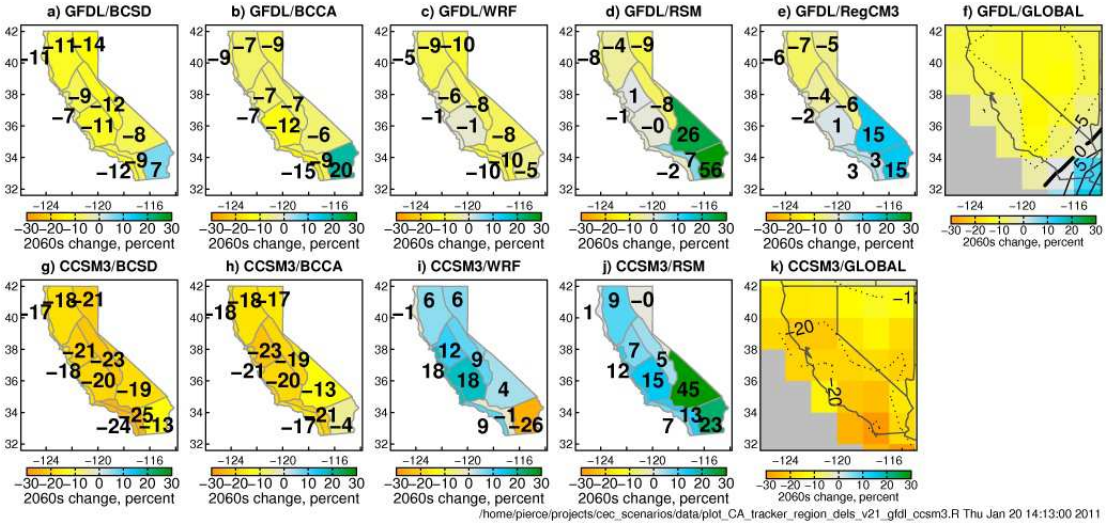

Figure 10. Yearly precipitation change (%, 2060-2069 compared to 1985-1994) from each downscaling technique applied to the GFDL 2.1 (top row) and CCSM3 (bottom row) global models. The yearly precipitation changes from the global models are shown in panels f and k, for comparison. Since the effect of downscaling on the global model fields is being illustrated, only one BCSD ensemble member is shown, the one corresponding to the illustrated global model and used for the dynamical downscaling.

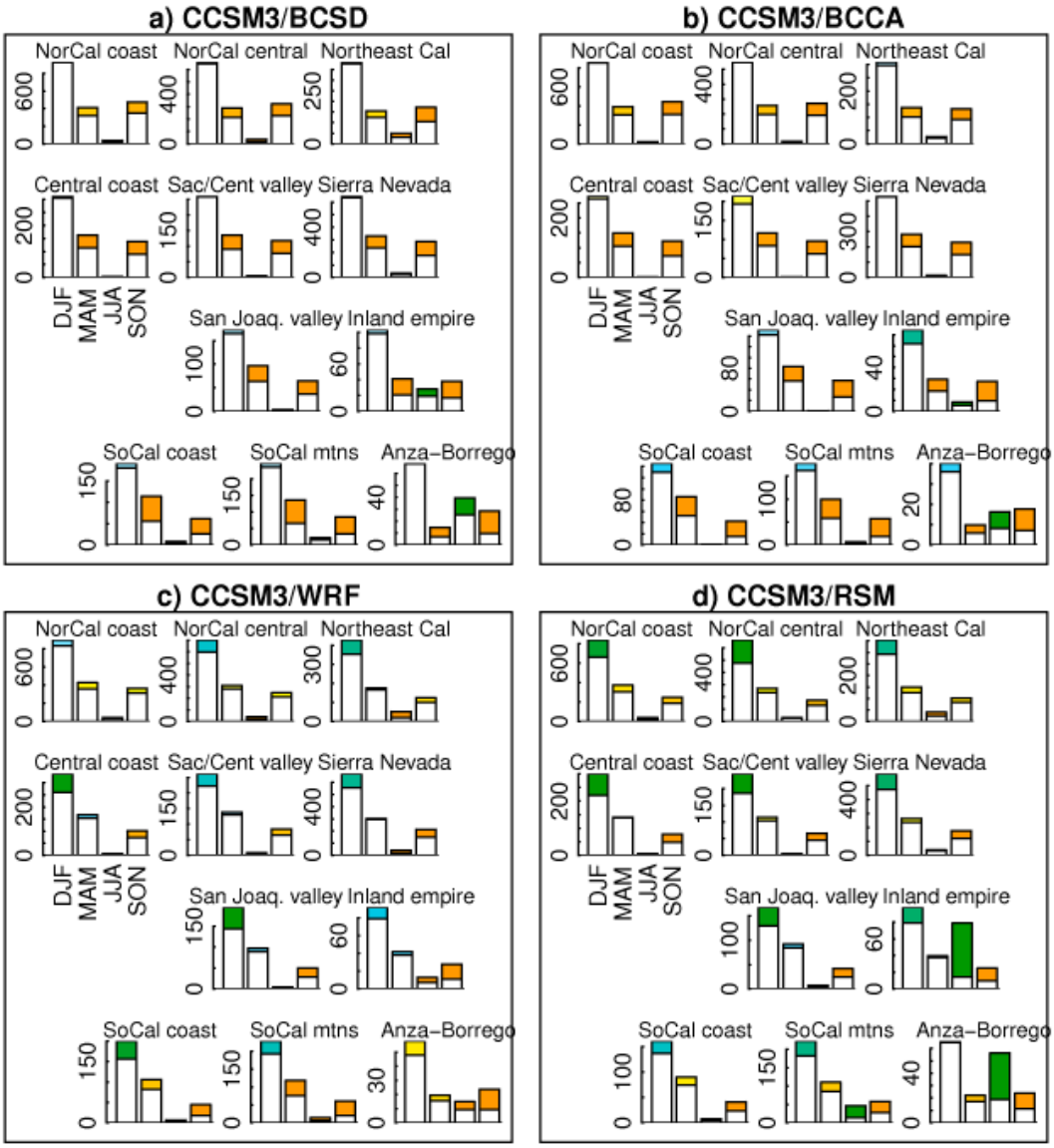

Figure 11. Changes in precipitation for the different downscaling methods applied to the CCSM3 global model. In each panel a-d, the subpanels show the precipitation changes by region, arranged roughly geographically. The bars show each region's seasonal precipitation (mm) in DJF, MAM, JJA, and SON (left to right) in the future and historical periods. The difference between the future and historical precipitation is colored, with the color determined by the percentage change using the same scale as Fig. 10 (yellows/oranges show less precipitation, blue/green show more precipitation). Note that every set of bars has a different Y axis, in mm.

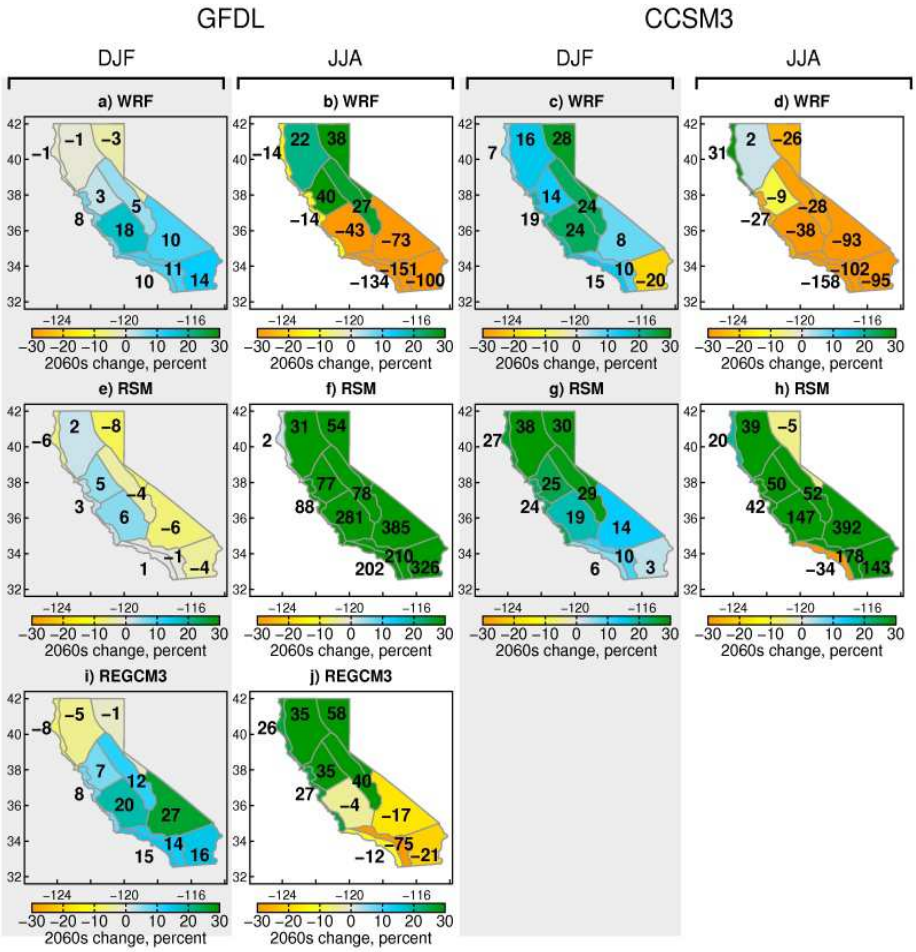

Figure 12. Difference (percentage points) between the change in seasonal precipitation projected by the dynamically downscaled simulations and the change found in the original global model (GFDL 2.1 or CCSM3, as labeled). Only winter (DJF) and summer (JJA) fields are shown.

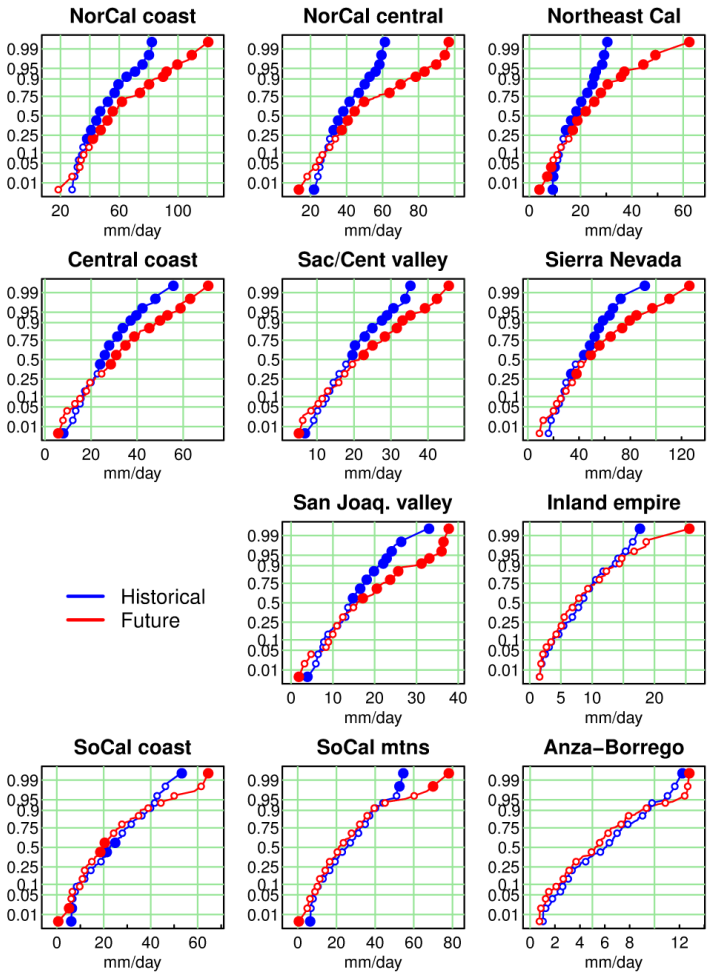

Figure 13. Cumulative distribution functions (CDFs) of the maximum 3-day mean precipitation in a calendar year. Regions are plotted roughly geographically. Y axis is probability (0-1) of experiencing the indicated average 3-day precipitation rate (mm/day), or lower. Large solid dots show where the two curves are different at the 95% significance level, evaluated using a bootstrap technique. Open circles indicate statistically indistinguishable values. Data from the 9 runs with daily data was used to make the figure.

747 **Supplemental Material for**

748 Probabilistic estimates of future changes in 749 California temperature and precipitation using 750 statistical and dynamical downscaling

751 David W. Pierce[1,*], Tapash Das[1,6], Daniel R. Cayan[1], Edwin P. Maurer[2], Norman
752 Miller[3], Yan Bao[3], M. Kanamitsu[1], Kei Yoshimura[1], Mark A. Snyder[4], Lisa C.
753 Sloan[4], Guido Franco[5], Mary Tyree[1]

754 1. Descriptions of the Regional Climate Models (RCMs)

755 *1.1 Regional Climate Model version 3 (RegCM3)*

756 RegCM3 is a third-generation regional-scale climate model derived from the
757 National Center for Atmospheric Research-Pennsylvania State (NCAR-PSU)
758 MM5 mesoscale model (Pal et al. 2007). RegCM3 has the same dynamical core as
759 MM5, the CCM3 radiative transfer package, and the Biosphere-Atmosphere
760 Transfer Scheme (BATS) land surface model (Dickinson et al., 1986; Giorgi et al.,
761 2003). RegCM has been validated against observations of modern-day climate in
762 multiple domains, and does well in simulating the spatial and temporal climate
763 features of California (Snyder et al. 2002, Bell et al. 2004). For this study
764 RegCM3 was configured with the Holtslag boundary layer scheme (Holtslag et
765 al., 1990), Grell cumulus scheme (Grell, 1993) with the Fritsch and Chappell
766 closure scheme (Fritsch and Chappell, 1980), and the Zeng (1998) ocean flux
767 parameterization. The model domain is centered over California with a horizontal
768 resolution of 10 km and 18 levels in the vertical.

769 *1.2 Weather Research and Forecasting model (WRF)*

770 We use a version of NCAR WRF version 3 coupled to the community land
771 surface model version 3.5 (CLM3.5; Oleson et al. 2004), referred to as "WRF-
772 CLM3" in Miller et al. (2009). The combination has an advanced land surface
773 scheme with sub-grid representation for snow and vegetation, lateral hydrologic

flow capability, and the potential for time-evolving plant functional types. The WRF model is set up with 10 km horizontal resolution, and uses the Kain-Fritsch convection parameterization for cumulus clouds (Kain and Fritsch 1993), the Yonsei University (YSU) planetary boundary layer (PBL) scheme (Hong and Pan 1996), and the Medium Range Forecast Model turbulence closure scheme (Mellor and Yamada 1982). The microphysics package used here is the WRF Single-Moment 3-class (WSM3) scheme (Hong et al. 2004), and the Rapid Radiative Transfer Model (RRTM) based on Mlawer et al. (1997) is used for describing longwave radiation transfer within the atmosphere and to the surface, and the shortwave scheme developed by Dudhia (1989). Dynamical downscaling using WRF has been evaluated over the state of California (Caldwell et al. 2009), and WRF coupled to CLM3.5 has been used to show that changes in vegetation can have appreciable effects on local climate (Subin et al. 2011).

1.3 Regional Spectral Model (RSM)

The version of the regional spectral model (RSM) used here is a development of the National Centers for Environmental Prediction (NCEP) global spectral model (GSM). The original regional code has been modified to have greater flexibility and increased efficiency (Kanamitsu et al., 2005). The RSM uses a two-dimensional spectral decomposition, and is implemented with so-called “spectral nudging”, i.e., relaxation towards the low-frequency components of the global simulation over the regional domain (Kanamaru and Kanamitsu 2007). The configuration used here is similar to that used to generate the 10-km California Reanalysis Downscaling (CaRD10) data set (Kanamitsu and Kanamuru, 2007). A scale-selective bias correction (SSBC) was used during these runs (Kanamaru and Kanamitsu 2007). The Noah land surface model with four soil layers was used, and cloud water and cloudiness are implemented as prognostic variables (Tiedtke 1993; Iacobellis and Sommerville 2000).

2. Statistical downscaling methods

We use two different statistical downscaling techniques. Both operate on bias-corrected GCM data; the bias correction (BC) procedure is described in section

804 2.3. The BCCA technique downscales daily global model data, while the BCSD
805 technique downscales monthly global model data.

806 *2.1 Bias Correction with Spatial Disaggregation (BCSD)*

807 BCSD (Wood et al. 2002, 2004) generates daily, fine-resolution ($1/8^o$ x $1/8^o$ in this
808 implementation) fields from monthly, bias-corrected GCM data by expressing
809 these coarse (GCM-scale) monthly values of average temperature and
810 precipitation as anomalies relative to a historical climatology. The monthly GCM
811 anomalies are interpolated onto the fine-scale grid, then applied, by offsetting (for
812 temperature) or scaling (for precipitation), to the long term mean at the fine scale.
813 This produces a fine scale monthly downscaled value. To generate daily
814 variability within each month an analogue month from the historical observations
815 is selected, with the selected month being the same month of the year as the data
816 being downscaled. The daily observed data for the analogue month on the fine-
817 scale grid is then offset (for temperature) or scaled (for precipitation) so that each
818 grid cell's monthly mean matches the monthly downscaled value. Since analogue
819 months from the historical period are used to generate the daily sequences, we do
820 not analyze BCSD-generated distributions of daily future climate variables. BCSD
821 downscaling is used, for example, by Hayhoe et al. (2004), Maurer (2007), and
822 Vicuna et al. (2007).

823 *2.2 Bias Correction with Constructed Analogues (BCCA)*

824 BCCA uses bias correction along with downscaling of daily GCM fields via
825 constructed analogues (Hidalgo et al., 2008; Maurer et al. 2010). BCCA is
826 therefore the CANA method described by Miller et al. (2009) along with a BC
827 step applied to the GCM temperature and precipitation fields. The constructed
828 analogue technique starts with a library of daily historical observations on a $1/8^o$ x
829 $1/8^o$ grid. This fine scale data is coarsened to the GCM grid, and the 30 best
830 matches (analogues) between the GCM fields for that day (including in the library
831 observed days within a ± 45 day window of the target date) and the coarsened
832 observations are computed. The 30 analogues are combined, using the strength of
833 their correspondence to the GCM grid as weights, into a GCM-sclae constructed

analogue. The same linear combination is then applied to the fine scale observed data to obtain the final downscaled data for a day.

3. Bias correction procedure

The output of the GCMs was bias corrected to observations (Maurer et al. 2002) before statistical downscaling, while the output of the dynamical RCMs was bias corrected after being generated. In general, before bias correction the RCMs tend to display 10-20% drier than observed conditions in the Northern part of the state in winter, 20-50% too wet conditions in the inland desert regions in winter, 10-20% wetter conditions than observed in the Northern part of the state in spring, and an overall warm bias of 0.1-2.0 C throughout the year.

BCSD starts with monthly GCM data, which we bias correct using the quantile-mapping technique (Panofsky and Brier, 1968), described in Maurer (2007), based on Wood et al. (2002, 2004). The mapping parameters are determined for each month by comparing the model results to the observations over the model/observations overlap period 1950-1999, and then are applied to the future period. The assumption is that the biases are unchanged in the future (cf. Liang et al. 2008). For bias correcting GCM output, Wood et al. (2004) suggest as long a historical period as possible be used to characterize monthly GCM biases, with ranges for robust error correction from 20-50 years (or longer). For temperature, the linear trend from the GCM output (interpolated to the fine scale grid) was removed at each point before the BC procedure was applied, and then added back in afterwards. The reason for this is explained by Wood et al. (2004): as temperatures rise in the future they are found more frequently outside the historic range, requiring excessive extrapolation during the quantile mapping. Precipitation, with typically much greater interannual variability than temperature, does not generally experience trends that exhibit this problem during remapping, so the trend removal and replacement was not applied. In theory, this procedure has the advantage that the final result preserves the original trend in the global model, but the disadvantage that the resulting trend is essentially that of the interpolated global model. In practice, the application of bias correction can still modify the original global model trends for reasons explained below.

The BCCA and RCM data are daily. We bias correct the daily data using a similar quantile mapping technique, described in Maurer et al. (2010). The historical period used for the monthly BCCA downscaling was the 50-yr span 1950-1999, but only the 10-yr period 1984-1995 is available for the RCM data. When bias correcting daily (instead of monthly) data, 10 years is adequate, as 10 years of daily information (~3652 time steps) provides considerably more samples than 50 years of monthly information (600 time steps) (Maurer et al., manuscript in preparation; see also Chen et al. 2011).

In contrast to BCSD, the global trend was not removed and then reapplied for the BCCA and RCM data, since the motivation for trend removal and replacement described above is not as strong for daily data. For example, since a large portion of the trend in daily temperatures is due to more frequent warm temperatures (as opposed to relatively few record hot temperatures) (Dettinger et al. 2004), which are represented in the historic period, the trend removal and replacement procedure is less necessary. This also means that the trend in these data sets is free to differ from the GCM trend. Since the basic assumption of downscaling is that it adds regionalized information to the global signal, this is a desirable characteristic.

However, the bias correction itself can modify the global trend (Hagemann et al. 2011). Table SM1 illustrates this for July average daily temperature at one grid point. Bias correction modifies the variance of the GCM output, since GCM simulations inevitably contain biases in variance, skew, and higher moments. The historical mapping is applied to future projections, so this process changes the statistical properties of the GCM projections. This table shows that when bias correction increases the standard deviation of the monthly data, then the low-frequency trend increases as well; when BC decreases the standard deviation, the trend decreases. In essence, the procedure assumes that errors in the amplitude of variability apply equally on all timescales, from daily to the secular trend. Whether the trend modification is appropriate given GCM errors in simulating variability or if the raw simulated trend should be preserved through the downscaling procedure is an open question.

4. Errors in the estimation of natural internal climate variability

The procedure described in the main text section 3.1.2 underestimates the value of natural internal climate variability since it is based the spread around the 10-yr average during the 2060's, but the 10-yr average itself will be affected by low-frequency natural internal climate variability. The size of this effect can be estimated from the historical record, assuming that future changes in the spectral structure of natural variability will be modest.

Using the technique described in Appendix A of Barnett & Pierce (2008) (transforming an observed time series to frequency space, randomizing the phases, and transforming back while taking sampling uncertainty in the estimate of the spectral amplitudes into account), we constructed 200 random time series for each variable (T, P) and each California region. Observed time series were computed from Hamlet and Lettenmaier (2005). Each random time series, by construction, has a mean and spectrum that is indistinguishable from observations (within sampling uncertainty). We then used the 200 random time series to calculate the natural variability as done in section 3.1.2 (in a 10-yr chunk) and compared it to the variability directly calculated from the full time series.

For temperature, the true 90% confidence interval was 6-20% wider than calculated as in the manuscript; for precipitation, the true 90% C.I. was 5-25% wider (Table SM2). This overstates the error in for temperature, since all California regions show a strong warming over the observed time period that has been shown to be anthropogenic in origin (e.g., Bonfils et al., 2008). Using a simple linear detrending for temperature and recomputing, the true C.I. for temperature was 6-14% wider than indicated by the method used in the manuscript. Figures 5 and 9 in the main text have been corrected to show this wider range for natural internal variability (the blue bars).

Supplemental Material References

Barnett TB, Pierce DW (2008) When will Lake Mead go dry? Water Resources Res 44:W03201 doi:10.1029/2007WR006704

925 Bonfils C, Santer BD, Pierce DW, Hidalgo HG, Bala G, Das T, Barnett TP, Cayan DR, Doutriaux
926 C, Wood AW, Mirin A, Nozawa T (2008) Detection and attribution of temperature changes in the
927 mountainous western United States. J Climate 21:6404-6424

928 Chen C, Haerter JO, Hagemann S, Piani C (2011) On the contribution of statistical bias correction
929 to the uncertainty in the projected hydrological cycle. Geophys Res Lett 38:L20403

930 Dettinger MD, Cayan DR, Meyer M, Jeton AE (2004) Simulated hydrologic responses to climate
931 variations and change in the Merced, Carson, and American River basins, Sierra Nevada,
932 California, 1900-2099. Clim Change 62:283-317.

933 Dickinson RE, Kennedy PJ, Henderson-Sellers A, Wilson M (1986) Biosphere-atmosphere
934 transfer scheme (BATS) for the NCAR Community Climate Model, Tech. Rep. NCAR/TN-
935 275+STR, National Center for Atmospheric Research

936 Dudhia J (1989) Numerical study of convection observed during the winter monsoon experiment
937 using a mesoscale two-dimensional model. J Atmo Sci 46:3077-3107

938 Fritsch JM, Chappell CF (1980) Numerical prediction of convectively driven mesoscale pressure
939 systems. part I: Convective parameterization. J Atmos Sci 37:1722–1733

940 Giorgi F, Bi XQ, Qian Y (2003) Indirect vs. direct effects of anthropogenic sulfate on the climate
941 of east asia as simulated with a regional coupled climate-chemistry/aerosol model. Clim Change
942 58:345–376

943 Grell G (1993) Prognostic evaluation of assumptions used by cumulus parameterizations. Mon
944 Wea Rev 121:764–787

945 Hagemann S, C Chen, JO Haerter, J Heinke, D Gerten, C Piani (2011) Impact of a Statistical Bias
946 Correction on the Projected Hydrological Changes Obtained from Three GCMs and Two
947 Hydrology Models. J Hydromet 12:556-578

948 Hamlet AF, Lettenmaier DP (2005) Production of temporally consistent gridded precipitation and
949 temperature fields for the continental United States. J Hydromet 6:330-336

950 Hidalgo HG, Dettinger MD, Cayan DR (2008) Downscaling with Constructed Analogues: Daily
951 precipitation and temperature fields over the Unites States. California Energy Commission
952 technical report CEC-500-2007-123. 48 pp.

953 Holtslag, AAM, de Bruijn EIF, Pan H-L (1990) A high resolution air mass transformation model
954 for short-range weather forecasting. Mon Wea Rev 118:1561–1575

955 Hong SY, Pan HL (1996) Nonlocal boundary layer vertical diffusion in a Medium-Range Forecast
956 Model. Mon Wea Rev 124:2322-2339

957 Hong SY, Dudhia J, Chen SH (2004) A revised approach to ice microphysical processes for the
958 bulk parameterization of clouds and precipitation. Mon Wea Rev 132:103-120

959 Iacobellis SF, Somerville RCJ (2000) Implications of microphysics for cloud-radiation
960 parameterizations: Lessons from TOGA COARE. J Atmos Sci 57:161-183

961 Kain JS and Fritsch JM (1993) Convective parameterization for mesoscale models: The Kain-
962 Fritsch scheme. Meteor Monogr No. 24, Amer. Meteor. Soc., 165-170.

963 Kanamaru H, Kanamitsu M (2007) Scale-selective bias correction in a downscaling of global
964 analysis using a regional model. Mon Wea Rev 135:334-350

965 Kanamitsu M, Kanamaru H, Cui Y, Juang H (2005) Parallel implementation of the regional
966 spectral atmospheric model. California Energy Commission technical report CEC-500-2005-014.
967 www.energy.ca.gov/2005publications/CEC-500-2005-014/CEC-500-2005-014.

968 Kanamitsu M, Kanamaru H (2007) Fifty-seven-year California Reanalysis Downscaling at 10 km
969 (CaRD10). Part I: System detail and validation with observations. J Clim 20:5553-5571

970 Liang XZ, Kunkel KE, Meehl GA, Jones RG, Wang JXL (2008) Regional climate models
971 downscaling analysis of general circulation models present climate biases propagation into future
972 change projections. Geophys Res Lett 35 doi:10.1029/2007GL032849

973 Maurer EP, Wood AW, Adam JC (2002) A long-term hydrologically based dataset of land surface
974 fluxes and states for the conterminous United States. J Clim 15:3237-51

975 Maurer EP, Brekke L, Pruitt T, Duffy PB (2007) Fine-resolution climate change projections
976 enhance regional climate change impact studies, Eos, Transactions, American Geophysical Union,
977 88:504, doi:10.1029/2007EO470006

978 Maurer EP, Hidalgo HG, Das T, Dettinger MD, Cayan DR (2010) The utility of daily large-scale
979 climate data in the assessment of climate change impacts on daily streamflow in California.
980 Hydrol. Earth Syst. Sci., **14**:1125-1138, doi:10.5194/hess-14-1125-2010

981 Mellor GL, Yamada T (1982) Development of a turbulence closure-model for geophysical fluid
982 problems. Rev Geophys 20:851-875

983 Miller NL, Jin J, Schlegel NJ, Snyder MA et al. (2009) An analysis of simulated California climate
984 using multiple dynamical and statistical techniques. California Energy Commission report CEC-
985 500-2009-017-F, August, 2009. 47 pp.

986 Mlawer EJ, Taubman SJ, Brown PD, Iacono MJ, Clough SA (1997) Radiative transfer for
987 inhomogeneous atmospheres: RRTM, a validated correlated-k model for the longwave. J Geophys
988 Res Atmos 102:16663-16682

989 Oleson KW, Dai Y, Bonan G, Bosilovichm M et al. (2004) Technical description of the
990 community land model (CLM). NCAR Tech. note NCAR/TN-461+STR. 186 pp.

991 Pal JS, Giorgi F, Bi XQ, Elguindi N et al. (2007) Regional climate modeling for the developing
992 world - The ICTP RegCM3 and RegCNET. Bull Amer Met Soc 88:1395

993 Panofsky HA. Brier GW (1968) Some Applications of Statistics to Meteorology, The Pennsylvania State
994 University, University Park, PA, USA, 224 pp.

995 Subin ZM, Riley WJ, Jin J, Christianson DS, Torn MS, Kueppers LM (2011) Ecosystem feedbacks
996 to climate change in California: Development, testing, and analysis using a coupled regional
997 atmosphere and land-surface model (WRF3-CLM3.5). *Earth Interactions*. 15: 1-38. doi:
998 10.1175/2010EI331.1

999 Tiedtke M (1993) Representation of clouds in large-scale models. Mon Wea Rev 121:3040-3061

1000 Wood AW, Maurer EP, Kumar A, Lettenmaier DP (2002) Long-range experimental hydrologic
1001 forecasting for the eastern United States. J Geophys Res Atmos 107 , doi:10.1029/2001jd000659

1002 Wood AW, Leung LR, Sridhar V, Lettenmaier DP (2004) Hydrologic implications of dynamical
1003 and statistical approaches to downscaling climate model outputs. Clim Change 62:189-216

1004 Zeng XB, Zhao M, Dickinson RE (1998) Intercomparison of bulk aerodynamic algorithms for the
1005 computation of sea surface fluxes using TOGA COARE and TAO data. J Clim 11:2628-2644

Table SM1

Statistic	NCAR CCSM3	CNRM CM3	NCAR PCM1	GFDL CM2.1
σ pre bias correction	0.84	0.66	0.49	0.73
σ post bias correction	0.67	0.85	0.50	0.60
ΔT pre bias correction	2.7	1.7	1.3	2.3
ΔT post bias correction	2.2	2.3	1.3	1.9

Table SM1. An example of the effect of bias correction on the standard deviation (σ) of average daily July temperature (for a future period of 2040-2069) on the projected changes in temperature (ΔT) between the future period and a historic baseline of 1950-1999 for a single grid point located at latitude 39, longitude -121, over northern California.

Table SM2

Region	a) T error	b) T error (detrended)	c) P error
S. California coast	20%	13%	9%
Anza-Borrego	8%	6%	25%
San Joaquin valley	14%	8%	9%
Sierra Nevada	7%	7%	5%
Northeast California	6%	8%	9%
N. California coast	18%	14%	6%
Central N. California	10%	10%	5%
Central coast	19%	8%	6%
S. California Mtns.	11%	9%	10%
Inland Empire	12%	7%	13%
Sac/Central Valley	19%	6%	9%

Table SM2. Estimated error in the 90% confidence interval of natural internal climate variability obtained when taking the average with respect to a 10-year period rather than using the entire period of record. Values are based on observations over the period 1915-2004. Column a) temperature; b) temperature, but detrending the temperature record first to remove anthropogenic warming; c) precipitation. See supplemental material text (section 4) for details.